Acta Biochim Biophys Sin 2024, 56(3): 474–481
https://doi.org/10.3724/abbs.2023289
Advance Access Publication Date: 19 January 2024
Original Article

Original Article

Arginine vasopressin induces ferroptosis to promote heart failure via activation of the V1aR/CaN/NFATC3 pathway

Zhiyong Wu[1,†], Hua Jiang[2,†], Qiulin Yin[1], Zhifeng Zhang[1], and Xuanlan Chen[1,*]

[1]Department of Cardiology, Jiangxi Provincial People's Hospital, the First Affiliated Hospital of Nanchang Medical College, Nanchang 330006, China, and [2]Department of Cardiology, Wuhan Asian Heart Hospital, Wuhan 430022, China
[†]These authors contributed equally to this work.
*Correspondence address. Tel: +86-791-87721357; E-mail: chenjhxl@163.com

Received 24 September 2023 Accepted 21 November 2023

Abstract

Arginine vasopressin (AVP) is a key contributor to heart failure (HF), but the underlying mechanisms remain unclear. In the present study, a mouse model of HF and human cardiomyocyte (HCM) cells treated with dDAVP are generated *in vivo* and *in vitro*, respectively. Hematoxylin and eosin (HE) staining is used to evaluate the morphological changes in the myocardial tissues. A colorimetric method is used to measure the iron concentration, Fe^{2+} concentration and malondialdehyde (MDA) level. Western blot analysis is used to examine the protein levels of the V1a receptor (V1aR), calcineurin (CaN), nuclear factor of activated T cells isoform C3 (NFATC3), glutathione peroxidase 4 (GPX4) and acyl-CoA synthase long chain family member 4 (ACSL4). Immunoprecipitation (IP) and luciferase reporter assays are performed to determine the interaction between NFATC3 and ACSL4. Both *in vivo* and *in vitro* experiments reveal that the V1aR-CaN-NFATC3 signaling pathway and ferroptosis are upregulated in HFs, which are verified by the elevated protein levels of V1aR, CaN, NFATC3 and ACSL4; reduced GPX4 protein level; and enhanced Fe^{2+} and MDA levels. We further find that inhibiting NFATC3 by suppressing the V1aR/CaN/NFATC3 pathway via V1aR/CaN inhibitors or sh-NFATC3 not only alleviates HF but also inhibits AVP-induced ferroptosis. Mechanistically, sh-NFATC3 significantly reverses the increase in AVP-induced ACSL4 protein level, Fe^{2+} concentration, and MDA level by directly interacting with ACSL4. Our results demonstrate that AVP enhances ACSL4 expression by activating the V1aR/CaN/NFATC3 pathway to induce ferroptosis, thus contributing to HF. This study may lead to the proposal of a novel therapeutic strategy for HF.

Key words arginine vasopressin, V1aR/CaN/NFATC3 pathway, ACSL4, ferroptosis, heart failure

Introduction

Heart failure (HF) is the end stage of most cardiovascular diseases and is a multifaceted and life-threatening syndrome that affects more than 64 million people worldwide [1]. The morbidity of HF is gradually increasing due to the aging of the population, and HF has become one of the major causes of mortality, poor quality of life, and high costs [2]. The clinical pathogenesis of HF is also complex and closely associated with the neuroendocrine system, ventricular remodeling and humoral factors [3]. Thus, decreasing the social and economic burdens of HF is a major global public health priority, and the exploration of novel pathological mechanisms and more effective prevention strategies are necessary.

Arginine vasopressin (AVP), also known as antidiuretic hormone, is involved in the regulation of body fluid balance and other functions via the receptor-G protein-second messenger pathway [4]. AVP has three receptors: V1aR, V1bR and V2R. V1a receptors are distributed mainly in vascular smooth muscle and the liver and are related to vasoconstriction and hepatic glycogenolysis; V1b receptors are located mainly in the pituitary gland and induce the secretion of adrenocorticotropin; and V2 receptors are located mainly in the distal convoluted tubules and collecting ducts of the kidney and promote water reabsorption [5,6]. After binding to the receptors, AVP exhibits its biological effects through a series of cascade reactions: V1a receptor activates phospholipase C by coupling with G protein to induce the release of intracellular calcium ions, thus affecting blood vessel constriction and liver glycogen decomposition [7]; V2 receptor activates guanylate-binding protein to increase the expression of aquaporin-2 in the

inner lining of renal collecting duct through cyclic adenosine-dependent pathway, and promotes the reabsorption of free water by the kidney [8]. It has been reported that AVP in myogenic cells activates the calcineurin (CaN) pathway through V1aR to affect the phosphorylation of downstream nuclear factor of activated T cells (NFAT), thus affecting the transcription of downstream regulatory genes [9]. It was also reported that the activated CaN-NFAT signaling pathway affects cardiac hypertrophy, and the transcriptional activation of NFAT family members regulates the central processes of HF [10]. Another study further revealed that adeno-associated virus-mediated deletion of NFAT family members could be used as a novel therapeutic strategy for HF [11]. However, the underlying mechanisms by which the NFAT family promotes HF remain unclear.

Ferroptosis is a new type of cell death that differs from other types of cell death in terms of mechanism and morphology, such as necrosis, apoptosis or autophagy [12]. Abnormal intracellular iron metabolism and lipid peroxidation are two indispensable and symbolic processes [13,14]. Ferrous iron provides free electrons via the Fenton reaction and further interacts with polyunsaturated fatty acids in cell membranes to produce lipid hydroperoxides, thus triggering cell death. Acyl-CoA synthase long chain family member 4 (*ACSL4*) is a key gene involved in ferroptosis that synthesizes arachidonic CoA and participates in membrane phospholipid synthesis [15]. In addition, ferroptosis reduces the expressions of antioxidant systems including glutathione (GSH) and glutathione peroxidase 4 (GPX4) [16]. Cardiomyocyte ferroptosis is closely associated with the occurrence and development of HF [17]. Several studies revealed that a reduction in ferroptosis improved isoproterenol-induced HF [18,19]. It has been reported that NFAT family members, NFAT5 and NFAT isoform 1 (NFATC1), bind to the *ACSL4* promoter region [20]. Bioinformatics prediction further revealed the binding sites between NFATC3/4 and *ACSL4*. Therefore, we speculated that the NFAT family may affect ferroptosis via the regulation of ACSL4. In addition, considering the involvement of AVP and the CaN/NFAT pathway in HF, we hypothesized that AVP may activate the CaN/NFAT pathway via V1aR to regulate ACSL4 expression, thus inducing ferroptosis and promoting HF.

In the present study, we not only analyzed the effect of AVP on HF but also explored the underlying mechanisms involved. This study might provide additional insights into the occurrence and development of HF and establish a novel therapeutic approach for HF patients.

Materials and Methods

HF model establishment

Male C57BL/6J mice (Cavins Laboratory Animals Co., Changzhou, China) aged 7–8 weeks were housed under standardized conditions with controlled temperature and humidity and a 12/12 h day/night light cycle. To induce the HF model, mice were ligated to the left anterior descending coronary artery. Mice were anaesthetized, the hair in the neck and left chest was removed, the surgical area was exposed, and the chest was opened between the third and fourth ribs to fully expose the heart. Then, a small amount of pericardium was collected, and the heart was quickly removed. A 6-0 suture needle was inserted into the lower margin of the left atrial appendage and passed through the left anterior descending coronary artery to completely block flow. After ligation, the heart was quickly reset, and the skin was sutured with a 6-0 suture needle. An increase in the electrocardiogram (ECG) ST section indicated successful establishment of the HF model. Mice in the Sham group only underwent thoracotomy and threading, without ligation. All the animal experiments in this study were performed following the Guide for the Care and Use of Laboratory Animals published by the U.S. National Institutes and approved by the Medical Ethics Committee of Jiangxi Provincial People's Hospital (No. KT090).

Hematoxylin-eosin staining

The paraffin-embedded myocardial tissues were dehydrated, cleared, wax-dipped, and embedded again. Then, the tissues were cut into 5-μm-thick sections with a microtome, and the sections were stained with hematoxylin and eosin according to standard protocol. Images were taken under a BX53 light microscope (Olympus, Tokyo, Japan).

Cell viability assay

Cell Counting Kit-8 (CCK8) assay was performed to examine the viability of human cardiomyocyte (HCM) cells. In brief, HCM cells were seeded into a 96-well plate and incubated at 37°C and 5% CO_2 for 24 h. Then, 10 μL of different concentrations of dDAVP (10^{-7}, 10^{-8}, 10^{-9}, or 10^{-10} M; Sigma, St Louis, USA) was added to the culture plate, and 20 μL of CCK8 reagent (Beyotime, Shanghai, China) was added to each well and incubated with the cells for 3 h in the dark. The optical density of each well was measured at 450 nm using a microplate reader (MK3; Thermo Scientific, Waltham, USA).

Western blot analysis

Proteins were extracted with RIPA buffer (Thermo Scientific), and the protein concentration was determined using a protein assay kit (Biosharp, Hefei, China). The proteins were separated by 10% SDS-PAGE and transferred to polyvinylidene difluoride membranes (Biosharp). The membranes were blocked with 5% skim milk (Wandashan, Harbin, China) and incubated with anti-GPX4 (ab125066, 1:2000; Abcam, Cambridge, UK), anti-ACSL4 (PA5-27137, 1:500; Invitrogen, Carlsbad, USA), anti-V1aR (MA5-18115, 1:2000; Invitrogen), anti-CaN (ab282104, 1:1000; Abcam), anti-NFATC3 (sc-8405, 1:1000; Santa Cruz Biotechnology, Santa Cruz, USA) and anti-β-actin (sc-8432, 1:1000; Santa Cruz Biotechnology) antibodies overnight at 4°C, followed by incubation with the secondary antibodies (ab7090, 1:1000; Abcam) for 1 h at room temperature. The protein bands were detected using Super ECL Plus detection reagent (ECL-0011; Dingguo Changsheng Biotechnology, Beijing, China).

Evaluation of iron level, Fe^{2+} concentration and MDA level

Colorimetric kits were employed to assess the total iron level (E-BC-K773-M; Elabscience, Wuhan, China), Fe^{2+} concentration (E-BC-K881-M; Elabscience) and MDA concentration (E-BC-K025-S; Elabscience) according to the manufacturer's instructions.

Immunoprecipitation assay

Immunoprecipitation (IP) assay was performed to analyze the interaction between NFATC3 and ACSL4. In brief, the cells were cross-linked with 1% formaldehyde and then homogenized. The homogenate was sonicated to generate short fragments of genomic

DNA. Then, equal amounts of treated chromatin were added to microwell plates (Costar, Cambridge, USA) containing the immobilized antibody for anti-NFATC3 (ab245501; Abcam). Crosslinked DNA was released from the antibody-captured protein-DNA complex, reversed, and purified through a Fast-Spin Column (Thermo Scientific). The purified DNA was subjected to PCR analysis. Briefly, the obtained DNA was amplified with specific primers, and the amplified products were subjected to agarose gel electrophoresis. Finally, the results were observed under ultraviolet lamp and photographed. The reaction conditions were as following: 5 min at 94°C; then 1 min at 94°C, 1 min at 55°C, and 2 min at 72°C for 40 cycles.

Luciferase reporter assay

ACSL4 containing the predicted wild-type (WT) or mutated (Mut) binding sites was amplified and cloned and inserted into the pGL2-control vector (Promega, Madison, USA) to construct ACSL4-WT and ACSL4-Mut. The ACSL4-WT/Mut constructs were co-transfected with NFATC3/NC (RiboBio, Guangzhou, China) into HEK293T cells (Sigma) using Lipofectamine 2000 (Invitrogen). Forty-eight hours after transfection, a Dual-Luciferase Reporter Assay Kit (Promega) was used to determine luciferase activity.

Statistical analysis

All the experiments were repeated three times ($n=3$). GraphPad Prism 7.0 was used to perform the statistical analyses. The differences between groups were analyzed using the unpaired Student's *t*-test or one-way analysis of variance (ANOVA). A *P* value less than 0.05 was considered statistically significant.

Results

HF mice exhibited activated V1aR/CaN/NFATC3 pathway and ferroptosis

To confirm the successful establishment of HF mice, we first assessed cardiac function of mice. We first observed significant increases in the left ventricular end-systolic diameter (LVDs) (Figure 1A) and left ventricular end-diastolic diameter (LVDd) (Figure 1B), as well as decreases in the left ventricular ejection fraction (LVEF) (Figure 1C) and left ventricular fraction shortening (LVFS) (Figure 1D), in HF mice. Additionally, HF mice exhibited

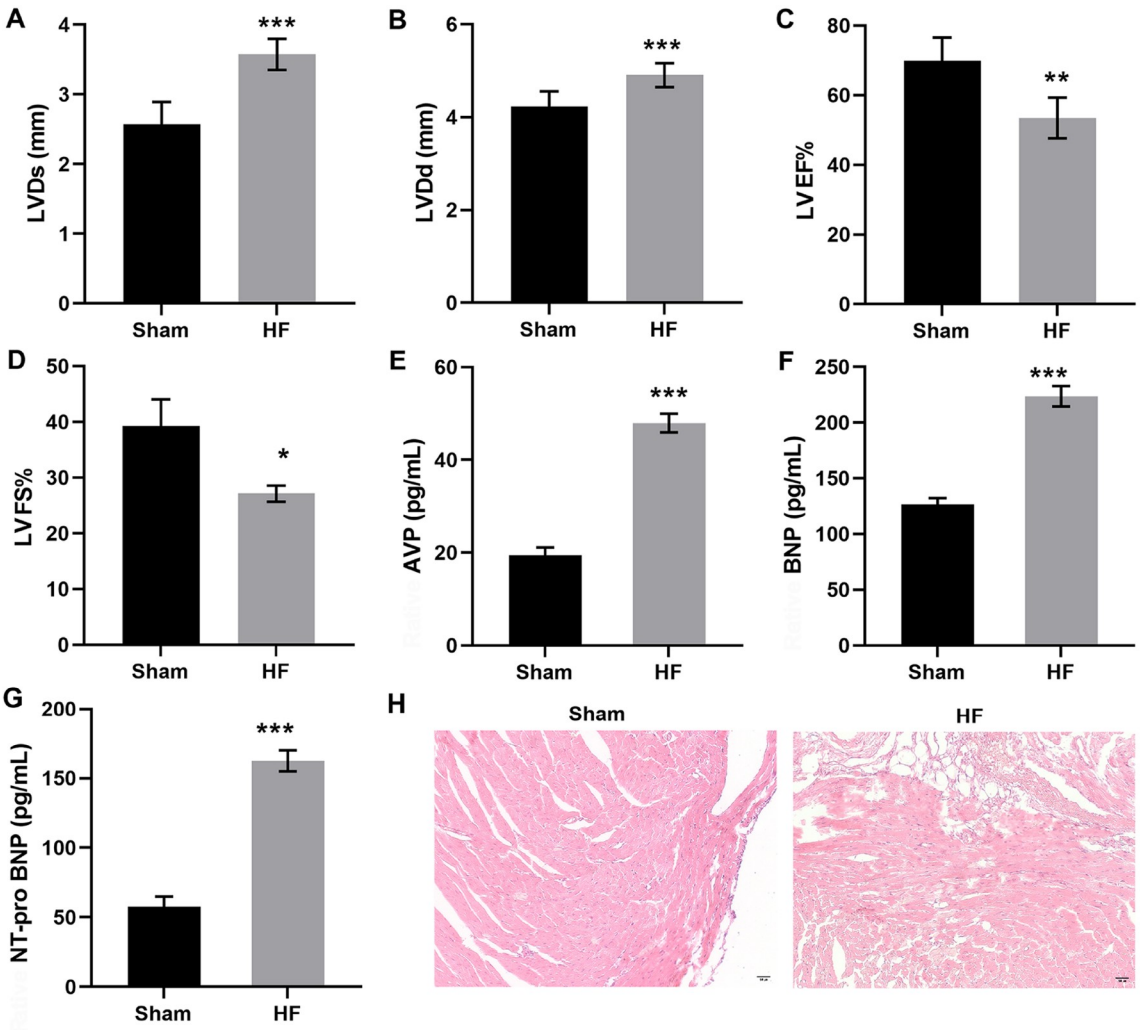

Figure 1. Assessment of HF mice A mouse model of HF was established, and LVDs (A), LVDd (B), LVEF (C), and LVFS (D) and serum AVP (E), BNP (F), and NT-pro BNP (G) were detected in mice from different groups. (H) HE staining was performed to assess the morphological changes in the myocardial tissues of mice (scale bar: 50 μm). Data are expressed as the mean ± SEM ($n=3$). *$P<0.05$, **$P<0.01$, ***$P<0.001$ vs the Sham group.

increased AVP (Figure 1E), brain natriuretic peptide (BNP) (Figure 1F), and NT-pro BNP (Figure 1G) in serum, compared to the sham group mice. HE staining further revealed evident pathological changes, such as cardiomyocyte fibrosis and inflammatory cell infiltration, in the myocardial tissues of HF mice (Figure 1H), indicating that the HF model was successfully constructed. In addition, elevated protein levels of V1aR, CaN, and NFATC3 were observed in the myocardial tissues of HF mice (Figure 2A–C). The HF mice also exhibited significantly enhanced ACSL4 protein level and reduced GPX4 protein level (a ferroptosis marker) in myocardial tissues (Figure 2A–C). Furthermore, the total iron and MDA levels were evaluated to assess ferroptosis. The results indicated that, compared with those in the sham group, the total iron level (Figure 2D) and MDA level (Figure 2E) were both obviously increased in the myocardial tissues of HF mice. These data indicated that HF mice exhibited activated V1aR/CaN/NFATC3 pathway and ferroptosis.

dDAVP activated V1aR/CaN/NFATC3 pathway and ferroptosis in HCM cells

Considering the increase in the protein level of V1aR in the myocardial tissues of HF mice, *in vitro* experiments were further performed to assess the effect of AVP on cardiomyocytes. dDAVP, a vasopressin analog, was used owing to its antidiuretic effects. CCK-8 assay revealed that treatment with dDAVP (10^{-9} M) markedly inhibited the proliferation of the HCM cells (Figure 3A). As expected, dDAVP (10^{-9} M) elevated the protein levels of V1aR, CaN, NFATC3, and ACSL4 but reduced the protein level of GPX4 (Figure 3B–D) in HCM cells. In addition, both the Fe^{2+} concentration (Figure 3E) and the MDA concentration (Figure 3F) were elevated in HCM cells treated with dDAVP (10^{-9} M). These data indicated that dDAVP activated the V1aR/CaN/NFATC3 pathway and ferroptosis in HCM cells.

Suppression of the V1aR/CaN/NFATC3 pathway reversed AVP-induced ferroptosis via direct interaction with ACSL4 in HCM cells

Next, we explored whether the V1aR/CaN/NFATC3 pathway participates in dDAVP-induced ferroptosis in HCM cells. HCM cells were pretreated with SR49059 (a V1aR inhibitor), CsA (a CaN inhibitor), or ferrostatin-1 (a ferroptosis inhibitor), followed by treatment with dDAVP. Both SR49059 and CsA obviously suppressed the V1aR/CaN/NFATC3 pathway by inhibiting V1aR, CaN and NFATC3 protein expressions (Figure 4A,B). We also found that dDAVP upregulated the ACSL4 protein level, Fe^{2+} concentration, and MDA level and reduced the GPX4 protein level; these changes were markedly reversed by SR49059, CsA, and ferrostatin-1 (Figure 4C–F). The binding sites between NFATC3 and ACSL4 was predicted by bioinformatics analysis (Figure 5A), and luciferase activity assays (Figure 5B) further confirmed the direct binding of NFATC3 to *ACSL4*. In addition, sh-NFATC3 was employed to suppress the V1aR/CaN/NFATC3 pathway by directly deleting the NFATC3 protein (Figure 5C). As expected, sh-NFATC3 and sh-ACSL4 had similar effects on the protein levels of GPX4 and ACSL4, the Fe^{2+} concentration, and the MDA level in HCM cells treated with dDAVP (Figure 5D–G). These data indicated that suppressed V1aR/CaN/NFATC3 pathway reversed AVP-induced ferroptosis via direct interaction with ACSL4 in HCM cells.

Suppression of the V1aR/CaN/NFATC3 pathway alleviated HF development by inhibiting ferroptosis

Finally, *in vivo* experiments were performed to assess the effect of the V1aR/CaN/NFATC3 pathway on ferroptosis in HF mice. HF mice were injected with SR49059, CsA or ferrostatin-1. SR49059, CsA and ferrostatin-1 all markedly reversed the changes in LVDs (Figure 6A), LVDd (Figure 6B), LVEF (Figure 6C) and LVFS (Figure 6D) in HF mice, and similar results were observed for serum BNP

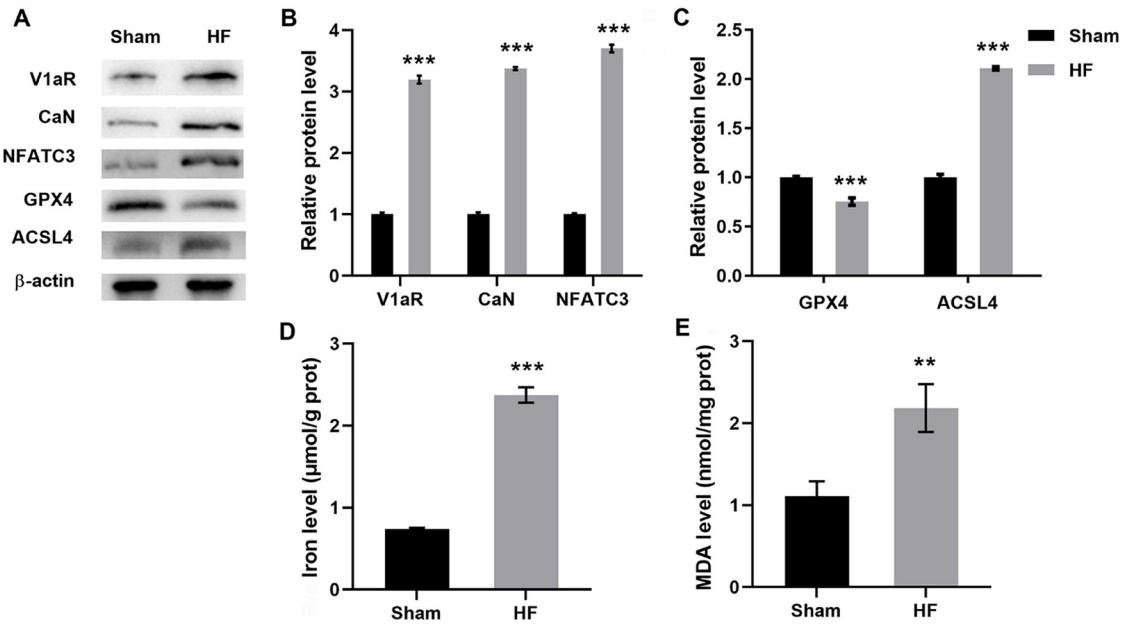

Figure 2. Detection of the AVP/CaN/NFATC3 pathway and ferroptosis in mice A mouse model of HF was established, and myocardial tissues were obtained from the mice for *in vivo* experiments. (A–C) Western blot analysis was performed to measure the protein levels of V1aR, CaN, NFATC3, GPX4 and ACSL4. A colorimetric kit was used to measure the iron level (D) and MDA level (E). Data are expressed as the mean ± SEM ($n = 3$). $^{**}P < 0.01$, $^{***}P < 0.001$ vs the Sham group.

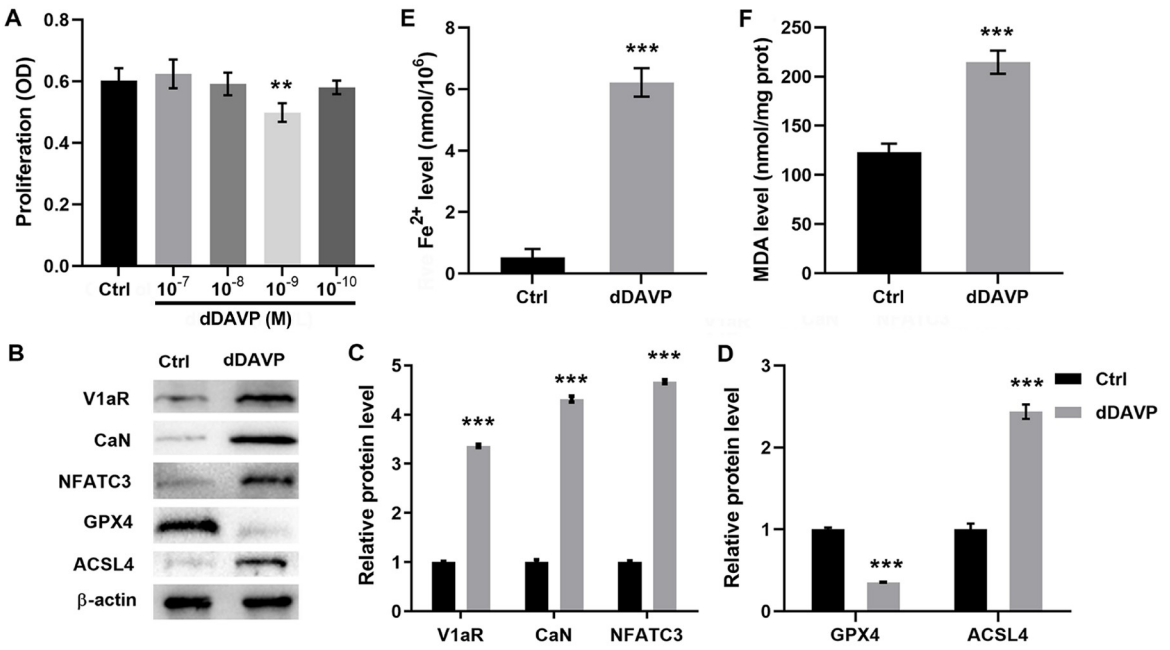

Figure 3. Detection of the AVP/CaN/NFATC3 pathway and ferroptosis in HCM cells HCM cells were used for the *in vitro* experiments. (A) CCK-8 assay was performed to assess the effect of different concentrations of dDAVP (10^{-7}, 10^{-8}, 10^{-9}, and 10^{-10} M) on cell proliferation. (B–D) Western blot analysis was performed to examine the protein levels of V1aR, CaN, NFATC3, GPX4 and ACSL4. A colorimetric kit was used to measure the Fe^{2+} concentration (E) and MDA level (F). Data are expressed as the mean ± SEM ($n = 3$). $^{**}P < 0.01$, $^{***}P < 0.001$ vs the Ctrl group.

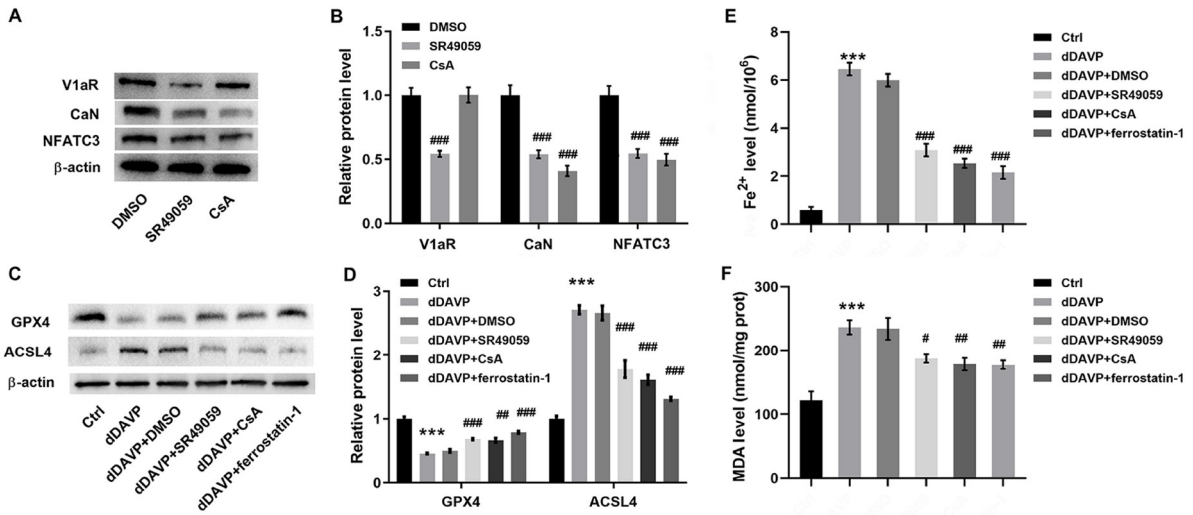

Figure 4. Effects of the AVP/CaN/NFATC3 pathway on ferroptosis in HCM cells HCM cells were used for the *in vitro* experiments. SR49059 (a V1aR inhibitor, 3×10^{-6} M), CsA (a CaN inhibitor, 1 μM) and ferrostatin-1 (a ferroptosis inhibitor, 1 mM) were used to inhibit the AVP-CaN-NFATC3 pathway. (A–D) Western blot analysis was performed to measure the protein levels of AVP, CaN, NFATC3, GPX4 and ACSL4. A colorimetric kit was used to measure the Fe^{2+} concentration (E) and MDA level (F). Data are expressed as the mean ± SEM ($n = 3$). $^{***}P < 0.001$ vs the Ctrl group; $^{\#}P < 0.05$, $^{\#\#}P < 0.01$, and $^{\#\#\#}P < 0.001$ vs the dDAVP + DMSO group.

(Figure 6E) and NT-pro BNP (Figure 6F). HE staining further showed that the evident pathological changes in the myocardial tissues of the HF mice were obviously attenuated in the HF + SR49059, HF + CsA and HF + ferrostatin-1 groups (Figure 6G). These data indicated that suppressing the V1aR/CaN/NFATC3 pathway alleviated HF development by inhibiting ferroptosis.

Discussion

Water and sodium retention are evident in advanced HF patients, and diuretics are largely applied to reduce load capacity in the clinic; however, long-term application of diuretics results in activation of the neuroendocrine system and damage to the kidney, and diuretic resistance is also a problem. AVP, a neuroendocrine mediator, is a key contributor to water and sodium retention in HFs. It was reported that the AVP concentration was obviously elevated in HF patients, and the degree to which AVP was elevated was proportional to the severity of HF [21,22]. AVP acts via three receptors: V1aR, V1bR and V2R. Here, we found that V1aR was

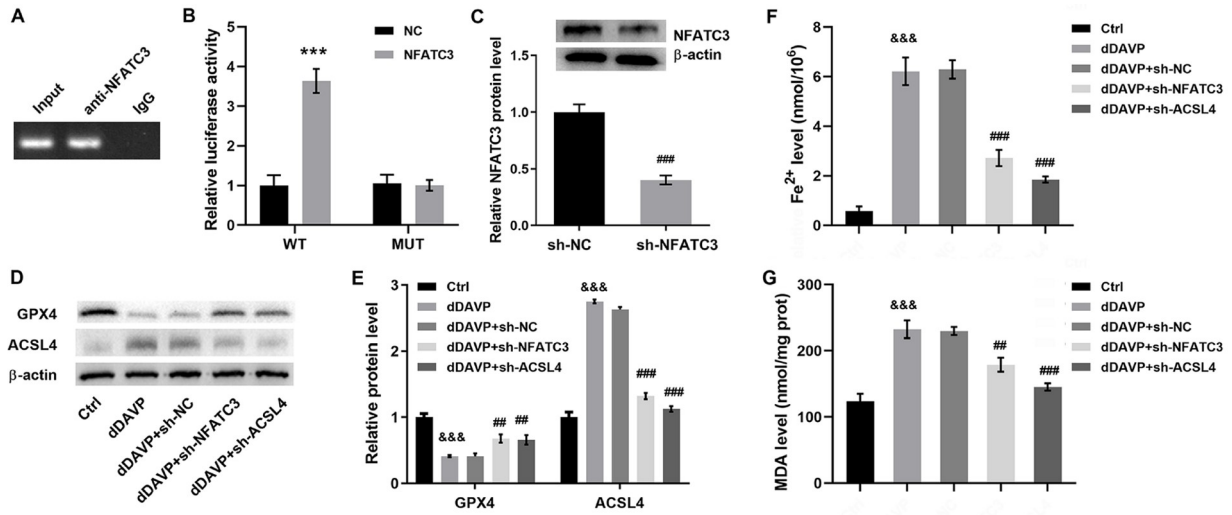

Figure 5. Effects of NFATC3 on ferroptosis in HCM cells HCM cells were used for the *in vitro* experiments. IP (A) and luciferase activity (B) assays were performed to evaluate the binding between NFATC3 and ACSL4. sh-NFATC3 and sh-ACSL4 were used to inhibit NFATC3 and ACSL4 expression, respectively. (C–E) Western blot analysis was performed to measure the protein levels of NFATC3, GPX4 and ACSL4. A colorimetric kit was used to measure the Fe^{2+} concentration (F) and MDA level (G). Data are expressed as the mean ± SEM ($n = 3$). $^{***}P < 0.001$ vs the NC group; $^{\&\&\&}P < 0.001$ vs the Ctrl group; $^{\#\#}P < 0.01$, $^{\#\#\#}P < 0.001$ vs the dDAVP + sh-NC group.

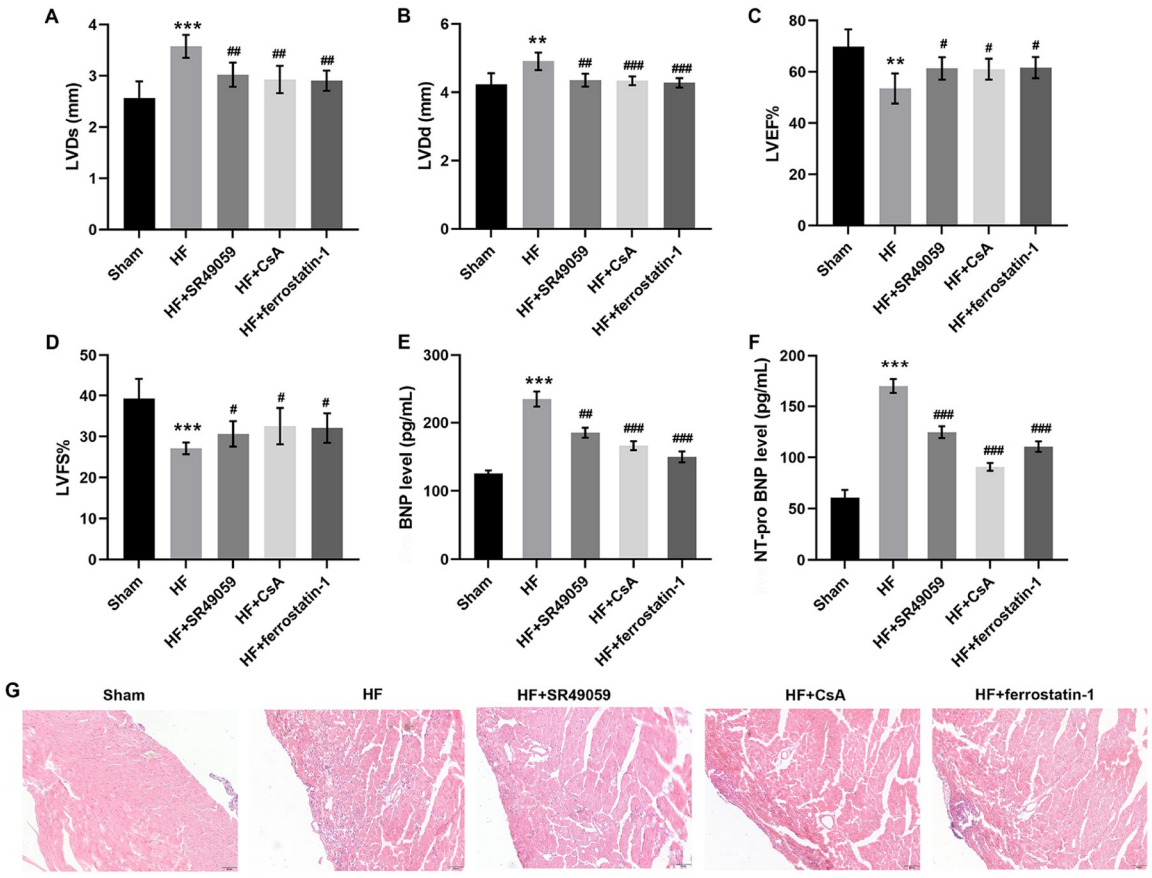

Figure 6. Effects of the AVP/CaN/NFATC3 pathway on HF mice A mouse model of HF was established, and HF mice were injected with SR49059 (tail vein injection, 2 mg/kg), CsA (tail vein injection, 50 mg/kg) or ferrostatin-1 (intraperitoneal injection, 5 mg/kg). The sham group mice received an equal volume of normal saline. LVDs (A), LVDd (B), LVEF (C), LVFS (D), serum BNP (E), and NT-pro BNP (F) were detected in mice from different groups. (G) HE staining was performed to assess morphological changes in the myocardial tissues of the mice (scale bar: 50 μm). Data are expressed as the mean ± SEM ($n = 3$). $^{**}P < 0.01$, $^{***}P < 0.001$ vs the Sham group; $^{\#}P < 0.05$, $^{\#\#}P < 0.01$, $^{\#\#\#}P < 0.001$ vs the HF group.

significantly increased in the myocardial tissues of HF mice, suggesting the involvement of the AVP/V1aR pathway in HF. The CaN-NFAT signaling pathway plays a key role in myocardial hypertrophy. Following dephosphorylation by CaN, transcriptional activation of the NFAT family members c1 to c4 regulates central processes in HF, such as extracellular matrix deposition and reactivation of the foetal gene program [23,24]. Many studies have delineated the importance of NFAT in cardiac hypertrophy. Activation of the CaN-NFAT pathway is sufficient to induce myocardial hypertrophy [25,26]. As expected, we also observed elevated protein levels of CaN and NFATC3 in the myocardial tissues of HF mice. Moreover, *in vitro* experiments further revealed that dDAVP markedly elevated the protein levels of V1aR, CaN and NFATC3 in HCM cells. Thus, based on the above results, we conclude that AVP activates the CaN/NFATC3 pathway via V1aR in HF.

In addition to exploring the role of the AVP/CaN/NFATC3 pathway in HF, the underlying mechanisms were also assessed. Generally, apoptosis is the major form of cell death, and researchers have found that cardiomyocyte apoptosis plays an important role in HF[27,28]. However, in addition to apoptosis, there may be other types of cell death in HFs. Ferroptosis is a type of iron-dependent programmed cell death that is involved in many diseases, such as neurodegeneration, inflammation, and ischaemia-reperfusion injury [29,30]. Recent studies have confirmed the link between ferroptosis and CVD and revealed that ferroptosis plays a major role in HF [17,31]. GPX4 is the key regulator of ferroptosis and is considered a marker of ferroptosis [32,33]. It has been reported that inhibition of GPX4 induces ferroptosis [34]. Here, we found that the GPX4 protein level was significantly reduced in both the myocardial tissues of HF mice and dDAVP-treated HCM cells. Iron promotes the production of superoxide radicals via the Fenton reaction, thus resulting in lipid peroxidation [35]. We further found that both iron and MDA levels were significantly increased in the myocardial tissues of HF mice, and similar results were obtained in *in vitro* experiments. All the above results suggest that ferroptosis is induced in HF.

Furthermore, the relationship between the AVP/CaN/NFATC3 pathway and ferroptosis in HF was also explored. Increasing evidence has revealed that ACSL4 acts as a biomarker and contributor to ferroptosis [36,37]. Bao *et al.* [38] reported that inhibition of ACSL4 suppressed ferroptosis in human glioblastoma cells. Cui *et al.* [39] reported that overexpression of ACSL4 promoted neuronal death by enhancing lipid peroxidation. In the present study, significantly elevated ACSL4 protein levels were also observed in the myocardial tissues of HF mice and dDAVP-treated HCM cells. Additionally, based on our bioinformatics prediction, the interaction between NFATC3 and ACSL4 was confirmed via IP and luciferase activity assays. Therefore, we wondered whether the AVP/CaN/NFATC3 pathway affects ferroptosis via the regulation of ACSL4 in HF. *In vitro* experiments revealed that inhibition of the AVP/CaN/NFATC3 pathway significantly suppressed ferroptosis, and deletion of ACSL4 produced similar results. Furthermore, inhibition of the AVP/CaN/NFATC3 pathway significantly improved cardiac function and pathological changes in the myocardial tissues of HF mice. Thus, we conclude that the AVP/CaN/NFATC3 pathway participates in HF development through the induction of ferroptosis via the regulation of ACSL4.

In summary, the findings of the present study demonstrated the involvement of the AVP/CaN/NFATC3 pathway in HF through the induction of ferroptosis, and the promotive effect of the AVP/CaN/NFATC3 pathway on ferroptosis is achieved by upregulating ACSL4 via direct binding of NFATC3 to ACSL4. This work provides novel insights into the mechanisms of the AVP/CaN/NFATC3 pathway in HF.

Funding

This work was supported by the grants from the Center for Diagnosis and Treatment of Difficult cases of the Cardiac System, the Jiangxi Provincial People's Hospital, the First Affiliated Hospital of Nanchang Medical College, and the Science and Technology Program of Health Commission of Jiangxi Province (No. 202130013).

Conflict of Interest

The authors declare that they have no conflict of interest.

References

1. Ao X, Ding W, Li X, Xu Q, Chen X, Zhou X, Wang J, *et al.* Non-coding RNAs regulating mitochondrial function in cardiovascular diseases. *J Mol Med* 2023, 101: 501–526
2. Pinar J, Pinarová L, Vítovec J. Pathophysiology, causes and epidemiology of chronic heart failure. *Vnitřní lékařství* 2018, 64: 834–838
3. Wehman B, Kaushal S. The emergence of stem cell therapy for patients with congenital heart disease. *Circ Res* 2015, 116: 566–569
4. Park KS, Yoo KY. Role of vasopressin in current anesthetic practice. *Korean J Anesthesiol* 2017, 70: 245–257
5. Nistor I, Bararu I, Apavaloaie MC, Voroneanu L, Donciu MD, Kanbay M, Nagler EV, *et al.* Vasopressin receptor antagonists for the treatment of heart failure: a systematic review and meta-analysis of randomized controlled trials. *Int Urol Nephrol* 2015, 47: 335–344
6. Iovino M, Iacoviello M, De Pergola G, Licchelli B, Iovino E, Guastamacchia E, Giagulli VA, *et al.* Vasopressin in heart failure. *Endocr Metab Immune Disord Drug Targets* 2018, 18: 458–465
7. Abel A, Wittau N, Wieland T, Schultz G, Kalkbrenner F. Cell Cycle-dependent coupling of the vasopressin V1a receptor to different g proteins. *J Biol Chem* 2000, 275: 32543–32551
8. Chandrashekhar Y, Prahash AJ, Sen S, Gupta S, Roy S, Anand IS. The role of arginine vasopressin and its receptors in the normal and failing rat heart. *J Mol Cell Cardiol* 2003, 35: 495–504
9. Sorrentino S, Barbiera A, Proietti G, Sica G, Adamo S, Scicchitano BM. Inhibition of phosphoinositide 3-kinase/protein kinase B signaling hampers the Vasopressin-dependent stimulation of myogenic differentiation. *Int J Mol Sci* 2019, 20: 4188
10. Khalilimeybodi A, Daneshmehr A, Kashani BS. Ca2 + -dependent calcineurin/NFAT signaling in β-adrenergic-induced cardiac hypertrophy. *Gen Physiol Biophys* 2018, 37: 41–56
11. Remes A, Wagner AH, Schmiedel N, Heckmann M, Ruf T, Ding L, Jungmann A, *et al.* AAV-mediated expression of NFAT decoy oligonucleotides protects from cardiac hypertrophy and heart failure. *Basic Res Cardiol* 2021, 116: 38
12. Th A, Brsa B. The development of the concept of ferroptosis. *Free Radical Biol Med* 2019, 133: 130–143
13. Doll S, Conrad M. Iron and ferroptosis: a still ill-defined liaison. *IUBMB Life* 2017, 69: 423–434
14. Liu Y, Ding W, Wang J, Ao X, Xue J. Non-coding RNA-mediated modulation of ferroptosis in cardiovascular diseases. *Biomed Pharmacother* 2023, 164: 114993
15. Guo N. Identification of ACSL4 as a biomarker and contributor of

ferroptosis in clear cell renal cell carcinoma. *Transl Cancer Res* 2022, 11: 2688–2699
16. Fanzani A, Poli M. Iron, oxidative damage and ferroptosis in rhabdomyosarcoma. *Int J Mol Sci* 2017, 18: 1718
17. Wu X, Li Y, Zhang S, Zhou X. Ferroptosis as a novel therapeutic target for cardiovascular disease. *Theranostics* 2021, 11: 3052–3059
18. Ning D, Yang X, Wang T, Jiang Q, Yu J, Wang D. Atorvastatin treatment ameliorates cardiac function and remodeling induced by isoproterenol attack through mitigation of ferroptosis. *Biochem Biophys Res Commun* 2021, 574: 39–47
19. Liu B, Zhao C, Li H, Chen X, Ding Y, Xu S. Puerarin protects against heart failure induced by pressure overload through mitigation of ferroptosis. *Biochem Biophys Res Commun* 2018, 497: 233–240
20. Dattilo MA, Benzo Y, Herrera LM, Prada JG, Castillo AF, Orlando UD, Podesta EJ, ***et al.*** Regulatory mechanisms leading to differential Acyl-CoA synthetase 4 expression in breast cancer cells. *Sci Rep* 2019, 9: 10324
21. Vinod P, Krishnappa V, Chauvin AM, Khare A, Raina R. Cardiorenal syndrome: role of arginine vasopressin and vaptans in heart failure. *Cardiol Res* 2017, 8: 87–95
22. Goldsmith SR. Arginine vasopressin antagonism in heart failure: current status and possible new directions. *J Cardiol* 2019, 74: 49–52
23. Schott P, Asif AR, Gräf C, Toischer K, Hasenfuss G, Kögler H. Myocardial adaptation of energy metabolism to elevated preload depends on calcineurin activity. *Basic Res Cardiol* 2008, 103: 232–243
24. Zarain-Herzberg A, Fragoso-Medina J, Estrada-Avilés R. Calcium-regulated transcriptional pathways in the normal and pathologic heart. *IUBMB Life* 2011, 63: 847–855
25. Molkentin J. Calcineurin-NFAT signaling regulates the cardiac hypertrophic response in coordination with the MAPKs. *Cardiovasc Res* 2004, 63: 467–475
26. Sankar N, deTombe PP, Mignery GA. Calcineurin-NFATc regulates type 2 inositol 1,4,5-trisphosphate receptor (InsP3R2) expression during cardiac remodeling. *J Biol Chem* 2014, 289: 6188–6198
27. Zhang Y, Chen B. Silencing circ_0062389 alleviates cardiomyocyte apoptosis in heart failure rats via modulating TGF-β1/Smad3 signaling pathway. *Gene* 2021, 766: 145154
28. Lai L, Xu Y, Kang L, Yang J, Zhu G. LncRNA KCNQ1OT1 contributes to cardiomyocyte apoptosis by targeting FUS in heart failure. *Exp Mol Pathol* 2020, 115: 104480
29. Zhang YH, Wang DW, Xu SF, Zhang S, Fan YG, Yang YY, Guo SQ, ***et al.*** α-Lipoic acid improves abnormal behavior by mitigation of oxidative stress, inflammation, ferroptosis, and tauopathy in P301S Tau transgenic mice. *Redox Biol* 2018, 14: 535–548
30. Pena-Bautista MCP, Vento M, Baquero M, Cháfer-Pericás C. Lipid peroxidation in neurodegeneration. *Clinica Chim Acta* 2019, 497: 178–188
31. Roetto A. Iron overload, oxidative stress, and ferroptosis in the failing heart and liver. *Antioxidants* 2021, 10: 1864
32. Ingold I, Berndt C, Schmitt S, Doll S, Poschmann G, Buday K, Roveri A, ***et al.*** Selenium utilization by GPX4 is required to prevent hydroperoxide-induced ferroptosis. *Cell* 2017: 423–434
33. Wang Y, Yang L, Zhang X, Cui W, Chen S. Epigenetic regulation of ferroptosis by H2B monoubiquitination and p53. *EMBO Rep* 2019, 20: e47563
34. Guan X, Li Z, Zhu S, Cheng M, Ju Y, Ren L, Yang G, ***et al.*** Galangin attenuated cerebral ischemia-reperfusion injury by inhibition of ferroptosis through activating the SLC7A11/GPX4 axis in gerbils. *Life Sci* 2020, 264: 118660
35. Sun X, Ou Z, Chen R, Niu X, Chen D, Kang R, Tang D. Activation of the p62-Keap1-NRF2 pathway protects against ferroptosis in hepatocellular carcinoma cells. *Hepatology* 2016, 63: 173–184
36. Yuan H, Li X, Zhang X, Kang R, Tang D. Identification of ACSL4 as a biomarker and contributor of ferroptosis. *Biochem Biophys Res Commun* 2016, 478: 1338–1343
37. Doll S, Proneth B, Tyurina YY, Panzilius E, Kobayashi S, Ingold I, Irmler M, ***et al.*** ACSL4 dictates ferroptosis sensitivity by shaping cellular lipid composition. *Nat Chem Biol* 2016, 13: 91–98
38. Bao C, Zhang J, Xian SY, Chen F. MicroRNA-670-3p suppresses ferroptosis of human glioblastoma cells through targeting ACSL4. *Free Radical Res* 2021, 55: 853–864
39. Cui Y, Zhang Y, Zhao X, Shao L, Liu G, Sun C, Xu R, ***et al.*** ACSL4 exacerbates ischemic stroke by promoting ferroptosis-induced brain injury and neuroinflammation. *Brain Behav Immun* 2021, 93: 312–321